Article

Additively Manufactured Wheel Suspension System with Integrated Conductions

Fabian Weitz *, Christian Simon Debnar, Michael Frey and Frank Gauterin

Institute of Vehicle System Technology, Karlsruhe Institute of Technology, 76131 Karlsruhe, Germany; christian.debnar@student.kit.edu (C.S.D.); michael.frey@kit.edu (M.F.); frank.gauterin@kit.edu (F.G.)
* Correspondence: fabian.weitz@kit.edu; Tel.: +49-721-60845362

Abstract: Increasing urbanisation and growing environmental awareness in society require new and innovative vehicle concepts. In the present work, the design freedoms of additive manufacturing (AM) are used to develop a front-axle wheel suspension for a novel modular vehicle concept. The development of the suspension components is based on a new method using industry-standard load cases for the strength design of the components. To design the chassis components, the available installation space is determined, and a suitable configuration of the chassis components is defined. Furthermore, numerical methods are used to identify the component geometries that are suitable for the force flow. The optimisation setup is selected in such a way that it is possible to integrate information, energy, and material-carrying conductions into the suspension arms. High-strength light metals are used to minimise the component masses. Apertures are provided through the components for the routing of electrical conductors. The transport of fluids is realised by conductions integrated into the wishbones. The final geometries of the suspension components are then validated by a finite element analysis (FEA) of the overall suspension model. The results of the applied method are lightweight suspension components with a high degree of functional integration. This improves the vehicle package and achieves higher front-wheel clearance, increasing the possible steering angles and thus improving manoeuvrability. The saving of unsprung mass can improve handling and has a positive effect on the vehicle's energy consumption. Furthermore, the sectional conduction integration is followed by a simplified assembly of the front-axle suspension.

Keywords: additively manufactured; wheel suspension; integrated conductions

1. Introduction

Efforts to achieve more sustainable mobility are driving the development of new types of vehicle concepts. The conservation of resources and minimisation of global warming are the central aspects of these efforts. The average operating time of passenger cars in Germany is only 45 min per day, and for the rest of the time, the vehicle stays unused in a parking space [1]. Consequently, there is great potential for increasing vehicle utilisation and the need to identify new utilisation concepts. These can significantly reduce greenhouse gas emissions per distance travelled. The following paper contributes to the U-Shift project. In this project, a modular vehicle concept is realised, which is based on an independent driverless driving module (driveboard) and various transport capsules (Figure 1). The driveboard contains all system components that are necessary for autonomous transport. The capsules are constructed as simply as possible and have few electronic components. In addition, capsules can be used for a variety of tasks, such as transporting people or goods. The special property of the project is the 'on-the-road' modularity, the ability of the driveboard to switch between different capsules during operation on the road. Technically, this is implemented by integrating a lifting device into the drive module. Ultimately, a high level of vehicle utilisation can be generated, especially when used in cities, by performing a wide variety of transport tasks.
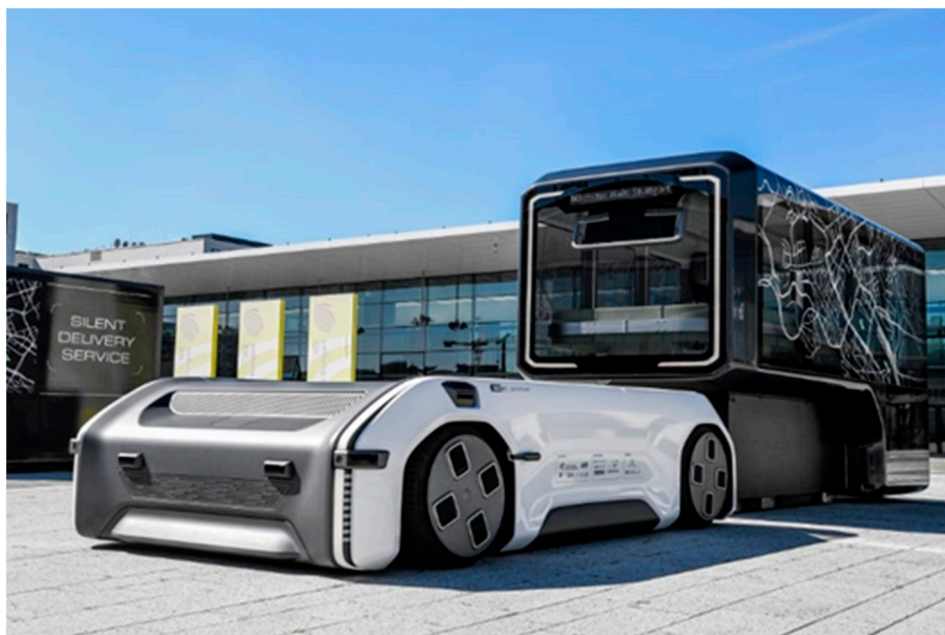
Figure 1. Driveboard (on the left) drives up to the passenger capsule (on the right) [2].

The ability to turn on the spot is required to enable changing of capsules within a limited space. With a steering angle of 73° in the opposite direction on the front axle, a vehicle turning around the centre of the rear axle is made possible. This results in high demands for the free movement of the front wheels. For the technical implementation of the concept, the use of new technologies, such as additive manufacturing, offers a lot of freedom in the design of the components. This enables the production of complex and multifunctional, lightweight components. The front-axle suspension components, in particular, benefit from increased functional integration due to the need to connect the wheel hub motors used to the on-board cooling water and hydraulic networks. In addition to the avoidance of installation space conflicts, a reduction in the total mass of the wishbones, wheel carrier, cooling water, and brake hoses required to operate the wheel hub motors is possible at the same time. This further reduces the energy required for driving during the utilisation phase.

The components presented in this paper are intended, on the one hand, to contribute to the optimisation of chassis systems with regard to the overall mass, including all conductions and attachments, and on the other hand, to save installation space and simplify assembly.

2. Materials and Methods

The front-axle suspension presented here is being developed for the prototype of the U-Shift project. The permissible total mass of the vehicle when using a passenger capsule is 5 t in total, which is over 270% above the mass of the empty driveboard. For vehicles with high axle loads and drive forces, double or multi-link front axles are often installed [3]. Due to the low maximum driving speed of 30 km/h, low demands are placed on the driving dynamics of the demonstrator. Consequently, the extended design freedoms of a multi-link front axle are not required, and a double-wishbone front axle can be used. The main requirements for the front-axle suspension are as follows [3]:

- First of all, the suspension must maintain the position of the wheel in relation to the body and the road in all driving situations and occurring forces in such a way that the vehicle guidance is not disturbed.
- It must have a high-pitch pole to allow sufficient brake pitch compensation.
- It must minimise the unwanted (lifting, tilting, and rolling) movements of the superstructure.
- It must transmit forces in such a way that the reaction time during acceleration, braking, and steering is very short (high stiffness).

- It must prevent the transmission of vibrations and shocks coming from the wheel.
- The design of the wheel suspension must take crash requirements into account. Attachment points on the longitudinal members must not hinder energy absorption.
- Axle components should deform plastically under high loads but not break. In this way, wheel guidance and steerability are maintained as far as possible, even in the event of misuse or accidents.
- The required wheel housing spaces, taking into account the largest possible steering angles for a small turning circle, are to be kept as small as possible within the scope of the vehicle package.
- For driven axles, it must offer sufficient free space around the centre of the axle for the side shafts and the differential.
- Disturbances due to torque fluctuations, brake disc tolerances, imbalances, ESP effects, and road roughness are to be kept away from the steering system.
- The steering kinematics must ensure a fast, even steering wheel reset.
- It must have understeering to neutral self-steering behaviour in the bends.
- The unequal friction coefficients on the left and right wheels must not interfere with the steering torque but support the driver as much as possible when levelling out.
- It must provide a direct feel of the road in all driving situations.

The design of the wheel suspension takes into account high loads from all spatial directions so that the safest possible vehicle handling is ensured, even in the event of misuse. In addition, the ductility and, thus, the energy absorption capacity of the components is increased through targeted post-heating treatment. Since the transverse links are not connected directly to the longitudinal links of the chassis but via stiff subframes, a selective weakening of the longitudinal links in the event of a crash is prevented. In addition, rubber bearings are used to transmit forces from the wishbones to the chassis subframe. These reduce the transmission of unwanted vibrations to the body. The position of the pitch pole is already determined by the position and orientation of the connection points of the wishbones to the subframe and is therefore assumed to be as follows: by a proper design of the spring-damper system, undesired body movements are damped. The stiffness of the chassis components that will be discussed in the following is maximised by using topology optimisation for the available design spaces with a given component mass so that the most direct driving behaviour possible is achieved. As a quality criterion for the component stiffness, it is specified that the connection points of the components may shift in relation to each other by less than 1.5 mm. The use of wheel hub motors leads to a clearly positive steering roll radius and also to a high space requirement. However, this is already taken into account in the design of the subframe, and therefore does not pose a problem. Since the vehicle has a long wheelbase and is only operated at low speeds, a negative steering roll radius, for example, to compensate for the μ-split, is not essential.

2.1. Additive Manufacturing

The additive manufacturing process selective laser melting (SLM) is chosen for the production of the chassis components. The reason for this is the good availability of the equipment, acceptable costs, and high component quality that can be achieved. In SLM, a thin layer of powder is applied to a build platform and melted locally by a laser, according to the layer information from the GCode. The build platform then moves down by one layer thickness in the z-direction, and another powder layer is applied. As the layer information is imprinted into the new powder layer, cohesion with the previous layer is simultaneously established. This process is repeated until a full component height is reached. After powder metallurgical production, the components are cleaned. If necessary, functional surfaces can be reworked by machining, and any support structures are removed. This results in components whose properties are comparable to those of the forged components [4]. In order to reduce residual stresses and to obtain almost completely dense components, thermal post-treatment can be used in conjunction with hot isostatic pressing [4]. Table 1 gives an overview of the constructive constraints of SLM.

Table 1. Design constraints in additive manufacturing using selective laser melting.

Feature Type	Limitation for Laser Powder Bed Fusion
Support angle	required from a downskin-angle $\geq 45°$ [4], $\geq 80°$ for small overhangs [5]
Wall thickness	≥ 0.3–0.5 mm [4], for ducts ≥ 1 mm [5]
Holes/tubes	≥ 0.5 mm diameter vertical, ≤ 8 mm diameter horizontal without support [4]
Minimum slot width	≥ 0.5 mm [4,5]
Screw threads	horizontally productible down to M4, must be tapped due to high surface roughness [4]

2.2. Design Space of Front-Axle Suspension Components

Table 2 summarises the geometric boundary conditions. The connection points to the subframe (Figure 2), the position of the wheel hub motor, and the connection point of the shock absorber to the lower wishbone are already given at the time of construction of the double-wishbone front axle presented.

Table 2. Geometric boundary conditions.

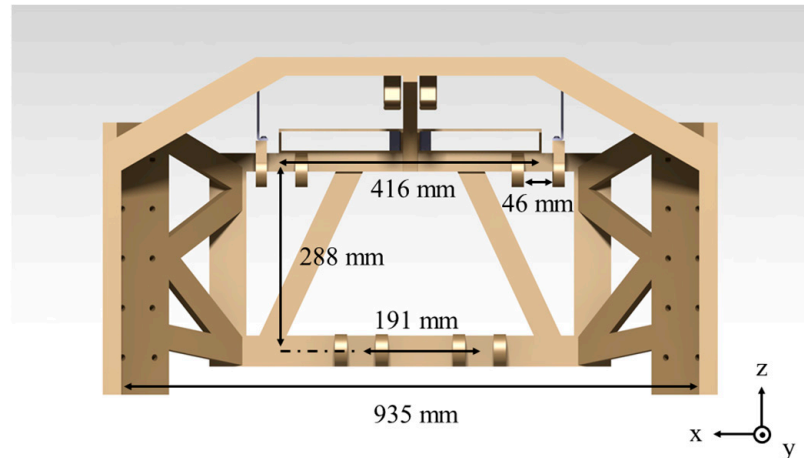| Boundary Condition	Quantity
Track width	2035 mm
Distance from subframe to wheel hub motor in y-direction	415 mm
Spring range in z-direction	150 mm
Steering angle (same direction)	$\pm 60°$
Steering angle (opposite direction)	$73°$

Figure 2. Side panel of the subframe in the wheel-side view with dimensions.

The arrangement of the chassis components takes into account that the intended bolted suspension joints have a significantly higher load capacity in the compression direction compared to the tension direction [6]. The available installation spaces for the individual components are initially determined based on the requirements for the kinematics to be mapped and the steering angles to be realised. However, the results of the topology optimisation are continuously analysed during the course of the development work, and the findings on the sub-areas critical for the component rigidity are thus incorporated into the installation space specification. Figure 3 shows the final design spaces available for the upper control arm, lower control arm, and wheel carrier components.
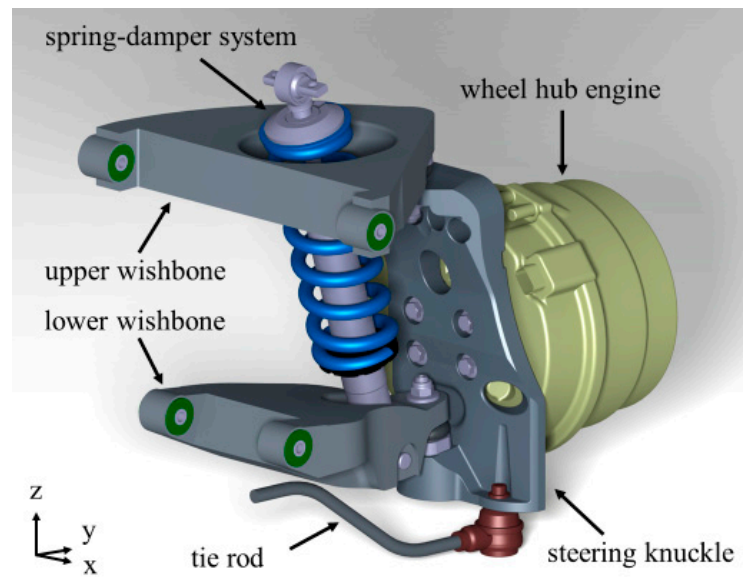
Figure 3. Representation of the design spaces for the front-axle suspension components.

2.3. Load Cases for Strength Design

First, the necessary load capacity of the wheel suspension is defined. In the automotive industry, the strength design of suspension components is commonly based on standard load cases (Table 3). The direction of acceleration refers to the transmission of force from the vehicle to the road. These are derived from driving manoeuvres and can be used for quasi-static FEA. The presented load cases 1 to 10 are used for quasi-static strength design, and the load cases 11 to 16 are used to verify the fatigue strength of chassis components. Since the load cases are expressed in terms of wheel accelerations, they can be applied to a wide range of vehicles [3]. The load cases Vertical impact (2), Longitudinal impact (3), and Lateral impact (4) represent high quasi-static loads on the chassis components in all spatial directions. The U-Shift prototype is intended for a low driving speed, but the selected load cases can also potentially occur at low speeds (attenuated). As the wheel accelerations represent limit cases that only rarely occur, the yield strength is used below as the material parameter for the mechanical design of the components. A check of the fatigue strength of the components is recommended when the components are pursued further.

Table 3. Standard load cases for the structural strength (Data taken from Ref. [3]).

	Standard Load Cases	Acceleration [g]		
		x	y	z
1	Sationary car	0.00	0.00	−1.00
2	Vertical impact 3.0 g	0.00	0.00	−3.00
3	Longitudinal impact 2.50 g	2.50	0.00	−1.00
4	Lateral impact 2.50 g	0.00	2.50	−1.00
5	Cornering right 1.25 g	0.00	1.25	−1.00
6	Braking while cornering	0.75	0.75	−1.00
7	Braking backwards 1.0 g	1.00	0.00	−1.00
8	Accelerate −0.5 g	−0.5	0.00	−1.00
9	Accelerating while cornering 0.7 g	−0.5	0.5	−1.00
10	Diagonal load	0.00	0.00	−1.75
11	Vertical spring in 2.25 g	0.00	0.00	−2.25
12	Vertical spring out 0.75 g	0.00	0.00	−0.75
13	Cornering right 0.75 g	0.00	0.75	−1.00
14	Cornering left 0.75 g	0.00	−0.75	−1.00
15	Braking 0.75 g	0.75	0.00	−1.00
16	Accelerate −0.5 g	−0.5	0.00	−1.00

Multiplying the wheel accelerations by the wheel load provides the forces at the wheel contact point acting on the vehicle. While 40% of the vehicle mass is on the front axle when the driveboard is empty, the proportion of the total mass on the front axle is reduced to 30% when the vehicle is fully loaded with a passenger capsule (Table 4).

Table 4. Axle loads on the front and rear axles.

Condition	Total Weight [kg]	Axle Load Front Axle [kg]	Axle Load Rear Axle [kg]
Empty Driveboard	1800	1080	720
Maximum load with personal capsule	5000	1500	3500

The maximum wheel load on the front wheel is 750 kg, according to Table 4. Since the unsprung masses are directly supported by the road surface, this can be neglected in the strength design of the double-wishbone front axle. The weight of the wheels, wheel hub motors, and other components proportionally belonging to the unsprung masses is 150 kg per wheel, which is a good approximation. Accordingly, the relevant proportion of the wheel load is set to 600 kg for the design of the chassis components. This assumption results in forces acting on the centre-wheel contact point, as shown in Table 5.

Table 5. Wheel induced forces.

	Standard Load Case	Wheel Induced Forces [N]		
		Fx	Fy	Fz
1	Vertical impact	0	0	17,658
2	Longitudinal impact	14,715	0	5886
3	Lateral impact	0	14,715	5886

2.4. Design of the Lower Wishbone

Based on the available installation space shown in Figure 3, topology optimisation of the lower wishbone was carried out in HyperWorks 2022. Since the lower wishbone is a component that is subjected to high bending stress, the light metal material Ti6Al4V is selected. This material combines high strength with low density and good corrosion resistance. Alternatively, stainless steel and nickel-based alloys are also suitable for the highly stressed component. Due to the high modulus of elasticity of the steels mentioned, a higher component stiffness can be achieved with the same available installation space. However, the simulation shows that the component mass is minimised by using Ti6Al4V, and the resulting displacements are acceptable. In order to allow the highest possible degree of plastic deformation, a thermal post-treatment of the wishbone is performed. Ti6Al4V has a yield strength of ≥970 MPa and a yield strength of ≥14% in all spatial directions after a two-hour heat treatment at 800 °C in a vacuum (Table 6). An additional post-treatment with HIP is helpful for increasing the fatigue strength of the components [4,7]. However, since the vehicle under consideration is a demonstrator designed for low mileage, this additional effort is not necessary.

Table 6. Typical properties of heat-treated additive manufacturing parts made of Ti6Al4V Grade 5 (Data taken from Ref. [7]).

Property		Vertical	Horizontal
Yield strength Rp0,2	[MPa]	1010	970
Tensile strength Rm	[MPa]	1080	1080
Elongation at break A	[%]	15	14
Reduction of area Z	[%]	≥25	≥25
Number of samples	[-]	84	72

The chassis components are optimised individually by determining the forces acting on the components using force and moment equilibria and applying them to the individual components via rigid body elements [8]. This procedure offers significant savings in computing time, as the individual components can be optimised with the help of a linear static model. The required safety against plastic deformation is already covered by the high requirements of the standard load cases. In order to sufficiently consider simplifications of the linear static optimisation setup of the individual components, a permissible maximum stress of 700 MPa is defined. This corresponds to a safety factor of 1.39, which exceeds the safety factor in the standard load cases. A final validation is carried out by a subsequent simulation of the overall model. The lower wishbone is used to guide the electrical conductors, which are necessary for the operation of the wheel hub motor. By optimising the component several times with different MINDIM settings (minimum member size), a component geometry is achieved that allows the conductors to pass through sensibly. This takes into account the recommendation from Altair Inspire, Inc. to select 3 to 12 times the average element size for the MINDIM setting. It is also possible to make MAXDIM (maximum member size) settings to further manipulate the resulting geometry. However, this is not done because it usually leads to poorer material utilisation [9]. The parameters used for the optimisation are summarised in Table 7.

Table 7. Parameters for topology optimisation of the lower wishbone.

Property	Quantity
Average element size	1.4 mm
Number of finite elements	2.2 mil
Material	Ti6Al4V
Stress constraint	700 MPa
Minimum member size	12 mm
Initial weight	15.26 kg
Mass fraction limit for design space	15%

Figure 4 shows the result of the topology optimisation. Due to the great design freedom of the AM, the force-flow-compatible component shape does not have to be reduced to simpler geometries as in conventional manufacturing, but only the design specifications discussed in the introduction have to be taken into account. In the following, the blue-coloured component areas represent the non-design volumes.
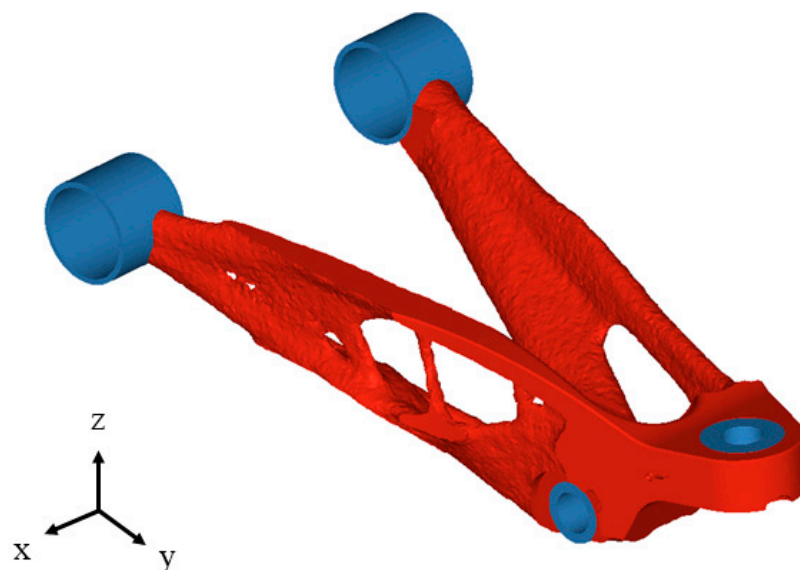

Figure 4. Result of the topology optimisation of the lower wishbone. Blue: non-design volumes.

The iso-surfaces of the design space are fed back into a common CAD (computer-aided design) format using the PolyNURBS tool integrated with Altair Inspire. The non-design areas are added manually. The final component is shown in Figure 5.
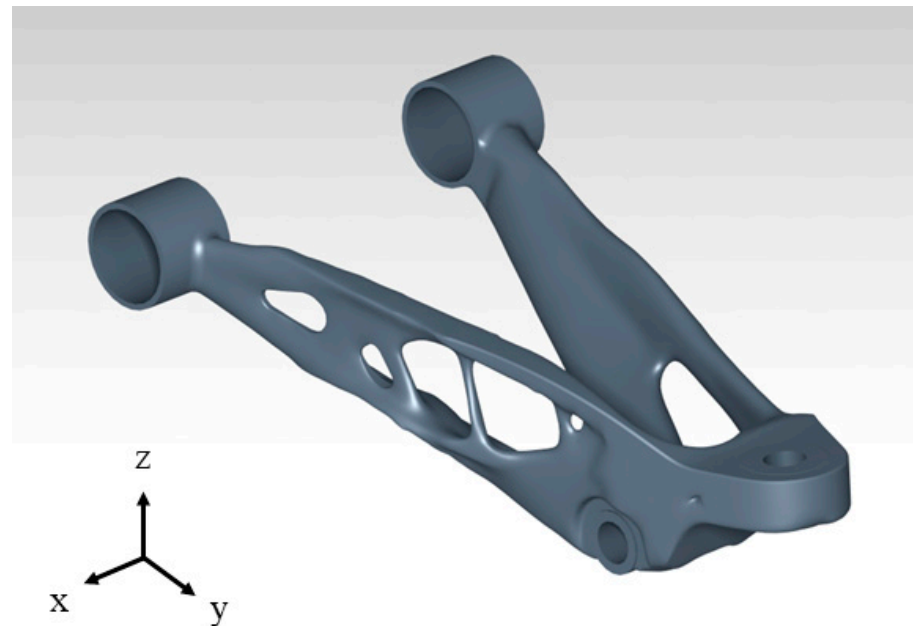

Figure 5. Final lower wishbone.

2.5. Design of the Steering Knuckle

The steering knuckle is exposed to high bending and torsional stresses. The component must be designed in such a way that no collisions occur between neighbouring components at the high steering angles required. Since the track width is limited and the position of the spreading axis is predetermined, a small component depth in the y-direction is available. Consequently, high-strength materials with the highest possible stiffness are also required. In analogy to the lower wishbone, it is checked whether the stiffness of Ti6Al4V is sufficient or whether the use of steel is required. Since the deformations of the connection points are acceptable when Ti6Al4V is chosen, and a low component mass is achieved by using this light metal, the titanium alloy is selected. The ductility of this material has already been discussed in the optimisation of the lower wishbone. The feed-throughs for information, material, and electrical cables are already planned in the design space. A recess is also required to allow the thread of the lower suspension joint to be recut. The optimisation of the topology focuses on improving the utilisation of the material. The parameters used for the optimisation are listed in Table 8.

Table 8. Parameters for topology optimisation of the steering knuckle.

Property	Quantity
Average element size	1.4 mm
Number of finite elements	1.9 mil
Material	Ti6Al4V
Stress constraint	700 MPa
Minimum member size	7 mm
Initial weight	8.53 kg
Mass fraction limit for design space	67%

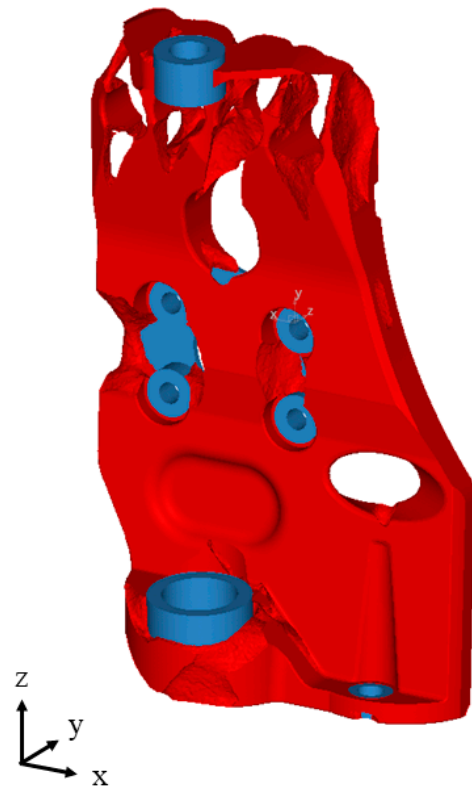As before, the optimised geometry (Figure 6) is fed back into a CAD model using a PolyNURBS tool (Figure 7).

Figure 6. Result of the topology optimisation of the steering knuckle, blue: non-design volumes.
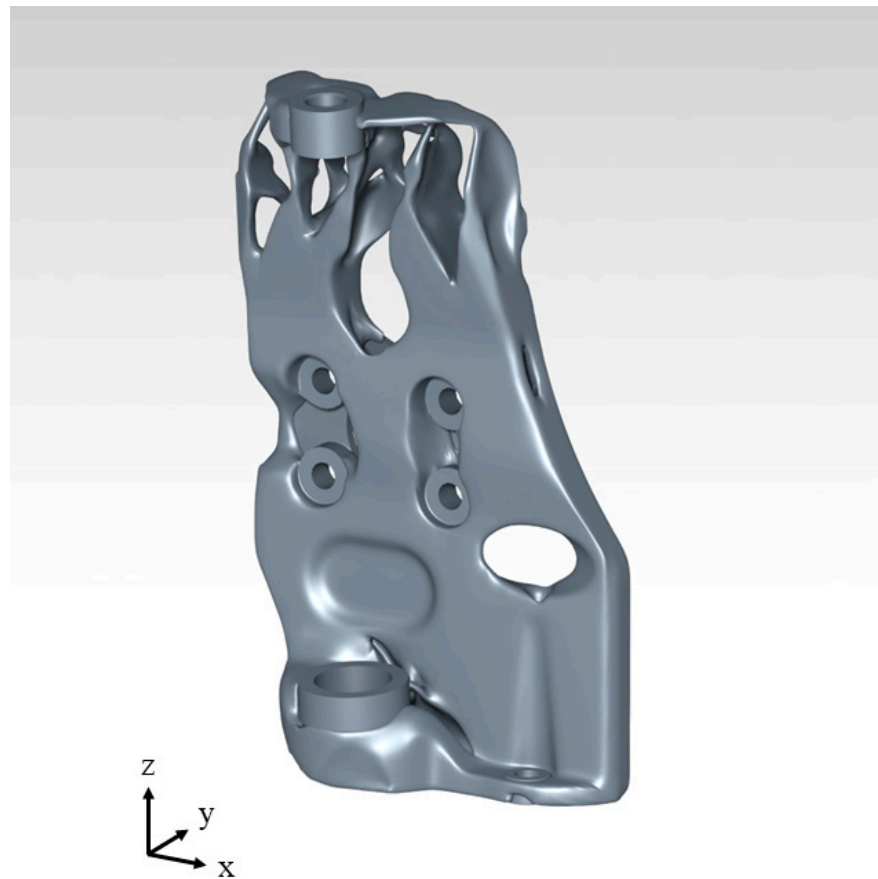

Figure 7. Final steering knuckle.

2.6. Design of the Upper Wishbone

The connections for the cooling water supply as well as the hydraulic connection of the brake system integrated in the wheel hub motor, are located at the upper part of the wheel hub motor. In order to avoid a collision between the connection hoses and the spring-damper system, the above-mentioned lines are integrated into sections into the upper wishbone. As the upper wishbone only has to support forces in the x- and y-directions, there is a significantly lower strength requirement for the material used than for the lower wishbone. Due to the high lightweight potential of aluminium alloys, the material AlSi10Mg, which is commonly used in powder metallurgy, was selected. This material has a high corrosion resistance, which is essential for contact with cooling water and brake fluid. In addition, the good thermal conductivity of aluminium provides a cooling effect on the fluids flowing through it. The disadvantage of the aluminium alloy is its low elongation at break in the as-built state. However, T6 heat treatment can increase the elongation at break to 10%, with a yield strength of $\geq$230 MPa (Table 9) [10].

Table 9. Typical properties of T6 heat-treated additive manufacturing parts made of AlSi10Mg (Data taken from Ref. [10]).

Property		Vertical	Horizontal
Yield strength Rp0,2	[MPa]	230	250
Tensile strength Rm	[MPa]	300	300
Elongation at break A	[%]	10	10

For a force-flow-compatible design of the component, topology optimisation of the design space is carried out as with the previously discussed components. At this point, the positions of the material-conducting lines remain undetermined. To minimise the component mass, the position of the lines is adapted to suitable force-flow paths. The maximum stress is initially set to 100 MPa, so that the topology optimisation already results in wide struts for subsequent line integration (Table 10).

Table 10. Parameters for topology optimisation of the upper wishbone.

Property	Quantity
Average element size	1.6 mm
Number of finite elements	1.2 mil
Material	AlSi10Mg
Stress constraint	100 MPa
Minimum member size	8 mm
Initial weight	7.65 kg
Mass fraction limit for design space	10%

As expected, an arrangement of tension and compression bars is suitable for transferring the imposed loads to the subframe. At the point of force application from the suspension joint to the wishbone, a stiffener is needed to support the bending moments (Figure 8).

It is analysed whether this optimised shape of the wishbone allows for a reasonable arrangement of material-carrying lines. Since a suitable line configuration is possible, the iso-surfaces from the optimisation are manually fed back into the CAD format in the PolyNURBS tool. A CAD environment is then used to model the lines in the component. In order to take into account the influence of the fluids flowing through, suitable fluid pressures must be specified for a design. The cooling water circuit is operated at a low pressure of well below 10 bar. To take into account an average safety factor of 1.5, a pressure of 15 bar is simulated on the cooling water channels. A maximum brake system working pressure of approximately 160 bar is often used to estimate deformations when designing brake systems. Pressure relief valves usually limit the system pressure to 204 bar [11]. To prove the strength of the wishbone, a pressure of 240 bar is applied to the brake line. This also corresponds to a safety factor of

1.5, which is also applied to this safety-relevant line, as further safety factors are included in the standard load cases and are also required in the validation of the overall model. This load spectrum is used to identify the weak points of the wishbone and to optimise it again manually. The final upper wishbone is shown in Figure 9.
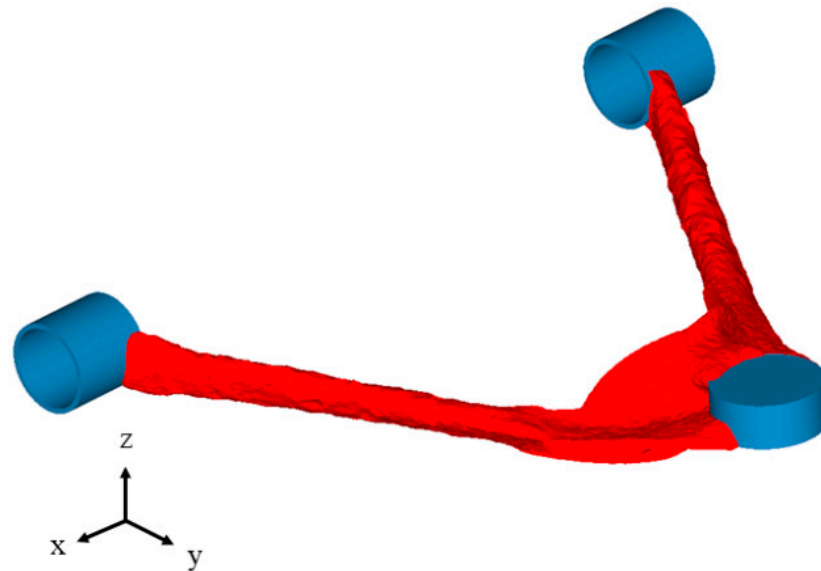

Figure 8. Result of the topology optimisation of the upper wishbone, blue: non-design volumes.
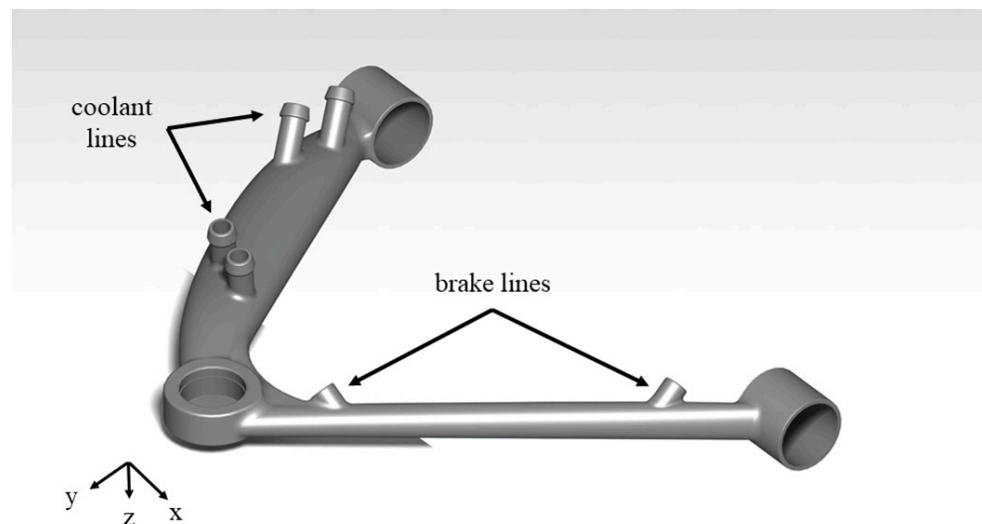

Figure 9. Final upper wishbone.

2.7. Validation

To save computing time, linear static models are used to optimise the individual components. The interfaces with the other components are simplified in this simulation. In addition, a change in the lever arms of the applied wheel forces due to large deformations of the components is not taken into account. In order to verify the structural strength of the entire system, it is necessary to use a non-linear quasi-static simulation model for large displacements. This also allows the modelling of component contacts. For the validation, a neutral wheel position is first used (Figure 10).
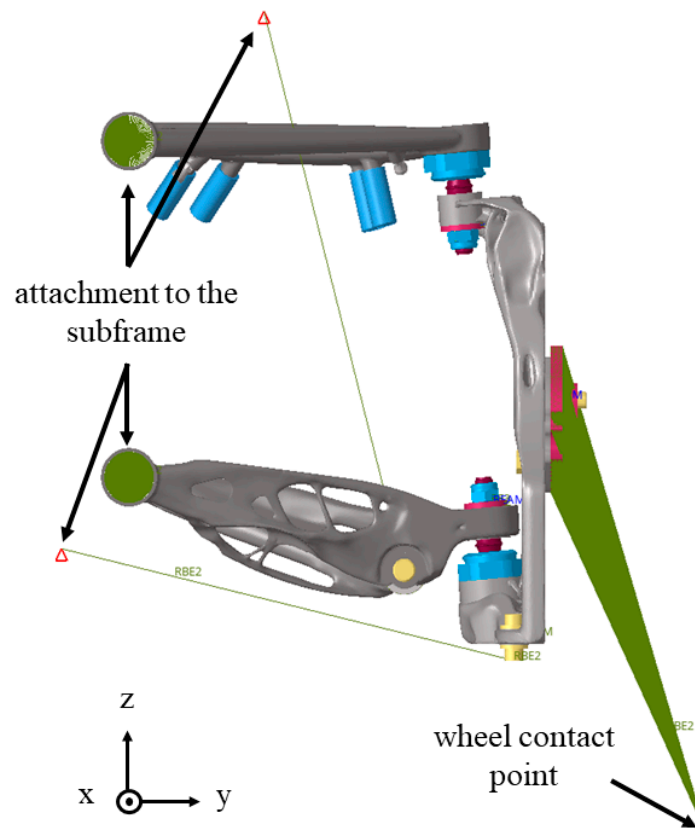
Figure 10. FEM model of the entire system.

Since only limited computing capacities are available, the components are divided into tetrahedral elements with a linear approach function (TETRA4). In order to achieve usable results despite the small number of nodes per element, an average element size of 1.5 mm is selected, which is small compared to the component dimensions. The overall model is discretised with a total of 4.15 million TETRA4 elements. The contact between the lower ball stud and the lower wishbone is modelled as a friction slide contact. This allows the lower wishbone to be pushed onto the ball stud, resulting in a radial preload in addition to the axial preload. The procedure for the ball stud of the upper suspension joint is analogous. The contact between the ball studs and the bearing sockets is also modelled as movable or frictional. The contacts of the screw heads to the adjacent components are modelled as rigid (no relative movement) to save calculation time since no relevant relative movement occurs if the screws are sufficiently pretensioned. The model contains a total of 21,953 surface-to-surface elements that represent the force transmission between the components. The shock absorber and track rod are substituted by rigid body elements, since the deformations of the AM components are to be investigated separately. For a realistic representation, however, the screwed connection elements are modelled. The point of application of the tyre forces from the standard load cases is represented by rigid body elements. These engage with a flange, which is used for a realistic connection of the wheel hub motor to the steering knuckle. In order to be able to represent the isotropic fluid pressures on the upper wishbone, dummy plugs are constructed for the cooling water and brake lines. In the first load case, a preload force is applied to the bolts and tapered connections. For this purpose, one-dimensional beam elements (1D-beams) are modelled (Figure 11). The choice of the preload force is based on empirical values and is selected iteratively according to the results from the simulation at 25 kN to 70 kN, depending on the connecting element [12]. In another load case, hydraulic pressure is applied to the upper wishbone. Based on the resulting displacements and stresses, the selected standard load cases are then simulated.
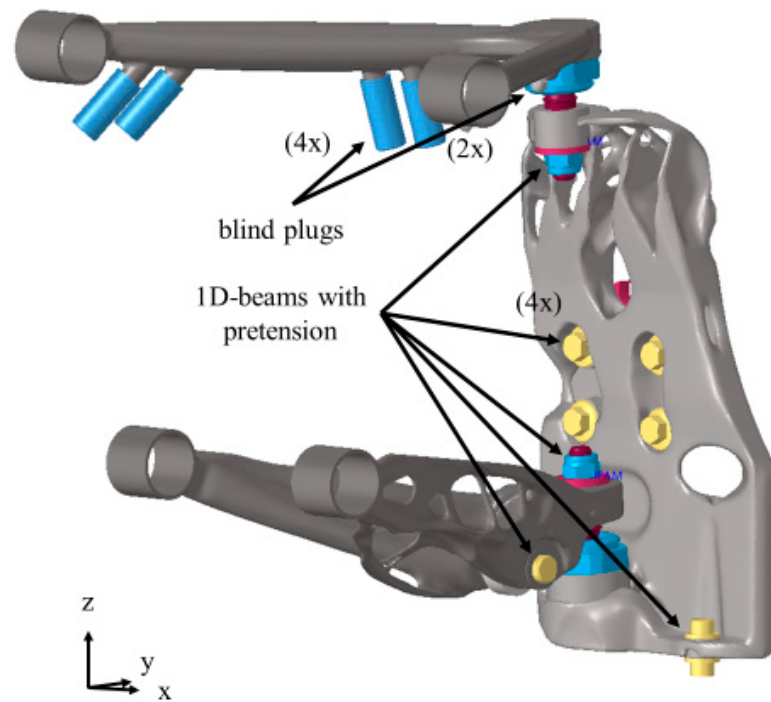
Figure 11. Preload of the screws and ball studs.

Based on the results of the simulation, final weak points and singularities can be identified, and then the stress peaks can be reduced constructively. The global displacements are shown in Figures 12–14 in the form of false-colour images. The fluid pressures are taken into account in the visualised deformations. The highest displacements occur in the standard load case (3) and longitudinal impact. This can be explained by the large lever arm in the y-direction due to the depth of the wheel hub motor. The large lever arm increases the effect of the tyre forces in the x-direction that occurs in the mentioned load case.
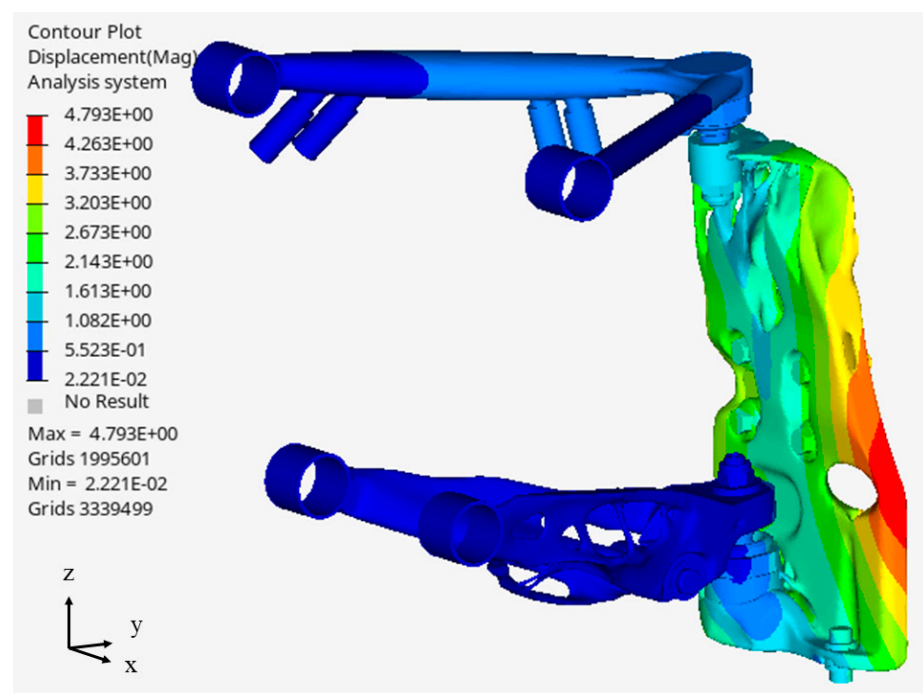
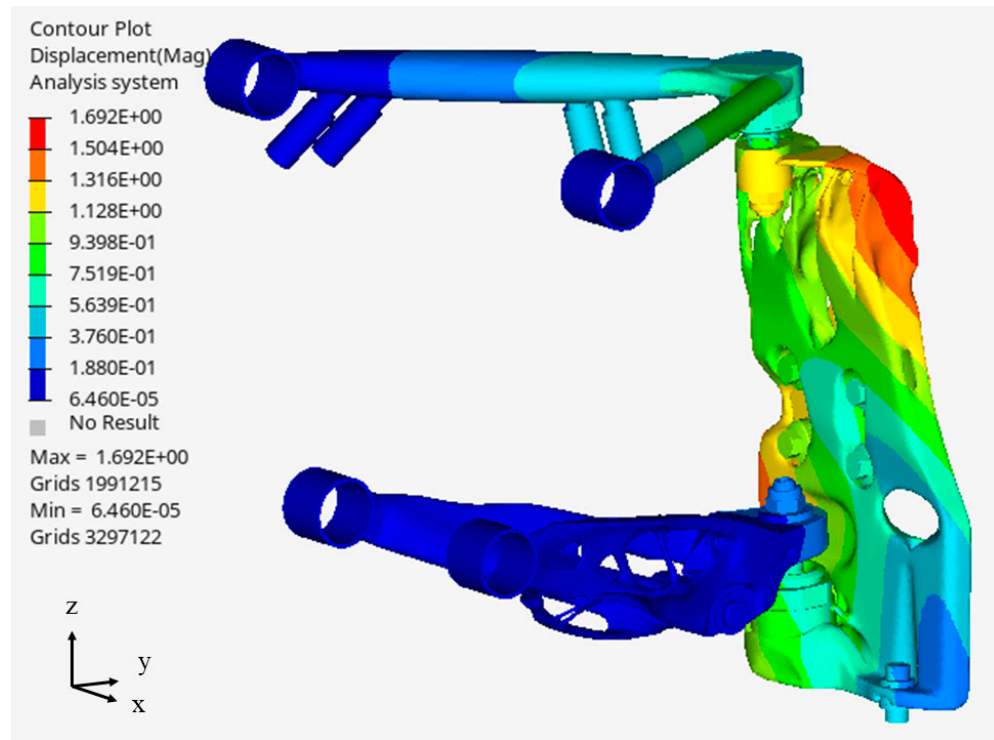**Figure 12.** Global deformations [mm] for standard load case longitudinal impact.

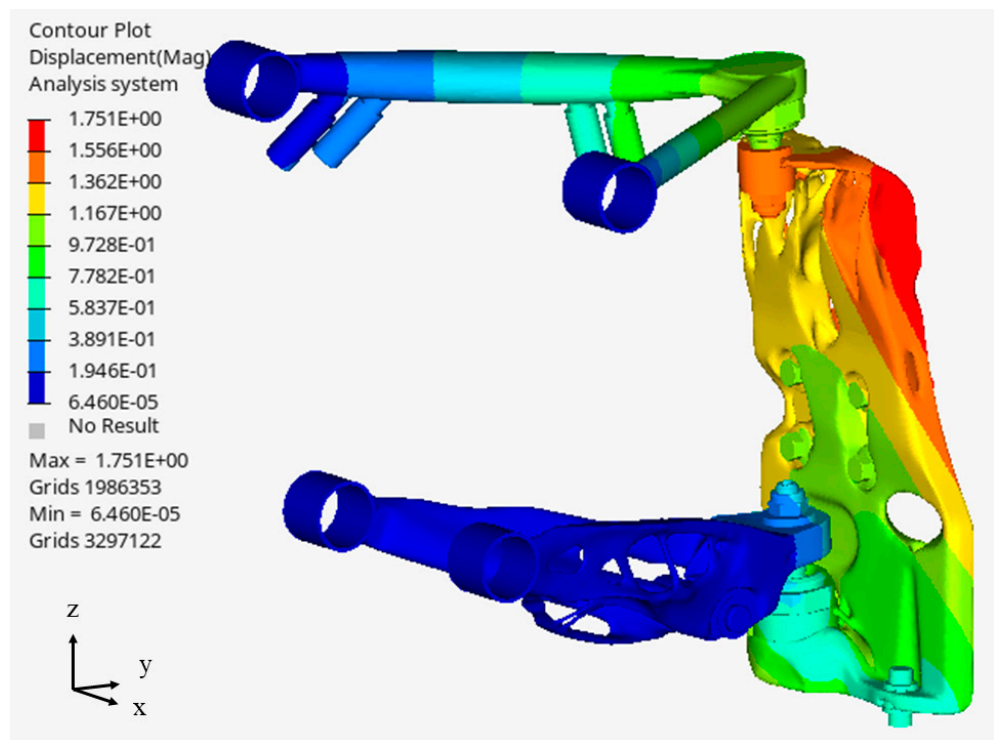**Figure 13.** Global deformations [mm] for standard load case lateral impact.

Figure 14. Global deformations [mm] for the standard load case vertical impact.

While the deformations of the wishbones are sufficiently small, large deformations of the steering knuckle occur, especially in the standard load case of longitudinal impact.

Figure 12 shows that these are areas of the components that are distant from the connection points. Consequently, these higher deformations are not passed on to the wheel and are therefore uncritical. The resulting deformation at the flange towards the wheel hub motor fulfils the quality criterion for the component stiffness defined in the introduction.

The uniaxial equivalent stress, according to Mises, is used to verify the structural strengths of the components. The quotient of the yield strength of the materials used and the occurring equivalent stress results in a degree of safety against plastic deformation, which goes beyond the safety contained in the load collectives. This safety covers, for example, simplifications in the FEM simulation and is, therefore, continuously marked S_{FEM}.

The maximum equivalent stress occurring in the steering knuckle, according to Mises, is 730.3 MPa (S_{FEM} = 1.33), and the maximum stress in the lower wishbone is 856.8 MPa (S_{FEM} = 1.13). These stresses occur in the standard longitudinal impact load case. Although these appear to be low safety factors, the design is still rated as load-bearing. The reason for this is that the longitudinal impact load case, which is particularly demanding for the chassis components, corresponds to a high acceleration of 2.5 g in the x-direction. As this general load case is designed for vehicles with a usually higher maximum driving speed, lower maximum accelerations can also tend to be expected at lower possible driving speeds. Thus, by conservatively retaining the standard load case, a higher level of safety is actually taken into account than the safety factor suggests. In order to support the assumptions made, it is recommended that the possible wheel accelerations on the real vehicle be recorded by sensors. The upper wishbone, on the other hand, is subjected to the greatest stress in the lateral impact. Here, it experiences a comparative stress of 123.8 MPa. (S_{FEM} = 1.85, Table 11). Simulated stresses for all components are below the yield strength of the materials used, and a small safety factor against simplifications is taken into account in the simulation so the components meet all strength requirements.

Table 11. Stresses, according to Mises, occurring in standard load cases.

Load Case	Stress [MPa]		
	Steering Knuckle	Lower Wishbone	Upper Wishbone
(2) Vertical impact	452.9	373.5	72.5
Vertical impact + hydraulic pressure	451.7	372.7	75.7
(3) Longitudinal impact	728.7	856.8	123.8
Longitudinal impact + hydraulic pressure	730.3	856.4	121.9
(4) Lateral impact	549.2	538.0	96.3
Lateral impact + hydraulic pressure	546.8	538.0	99.6

The selection of suspension joints is based on the loads derived from the force and moment balances, which are also used to optimise the single components. The selection of the joints is additionally validated by the FEM simulation of the entire model. The ball stud is identified as a critical component of the suspension joints. It is made of precipitation-hardenable stainless steel with a yield strength of 1550 MPa. The component experiences the highest stress in the standard load case longitudinal impact. Here, a comparative stress according to Mises of 1081 MPa occurs, resulting in a safety factor S_{FEM} of 1.43 (Figure 15). The exact stress values must be critically scrutinised, as there is always a deviation from the true stresses due to simplifications in the approach functions, the discretisation, and the numerical solution of differential equations in the FEA. In order to validate the simulation results, the aim is to investigate the convergence of the stress values in more detail as the project progresses.
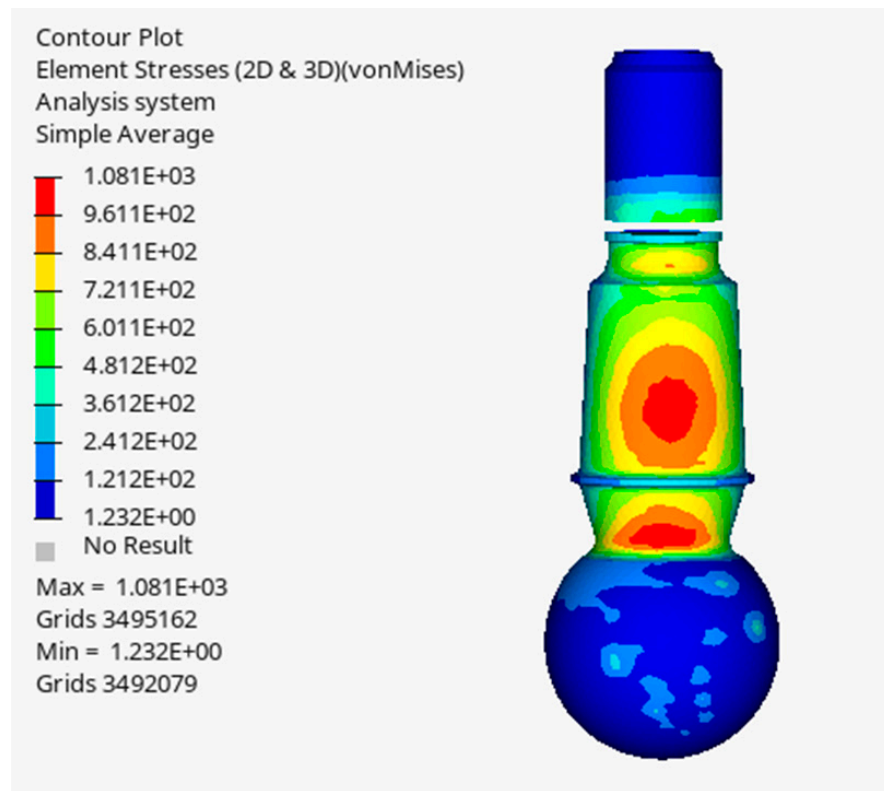
Figure 15. Stress conditions according to Mises [MPa] of the lower ball stud in the standard load case longitudinal impact.

3. Results

Figures 16 and 17 show the entire system consisting of the previously optimised chassis components. In particular, the routing of the high-voltage and low-voltage lines, as well as the cooling and brake lines, can be viewed in these figures.

The high-voltage lines for the wheel hub motor largely run through the installation space available for the lower wishbone and are protected from external influences by this. The sectional integration of the brake line into the upper wishbone prevents it from being damaged by contact with the wheel at high steering angles. This applies in the same way as to the cooling water lines. As a result of the airflow through the wheel housing, a cooling effect on the fluids is expected, especially since the aluminium used has a high thermal conductivity. Table 12 shows the resulting component weights. A conventionally manufactured front-axle suspension made of S460 is available for the prototype of U-Shift. The total weight of the wishbones and steering knuckles without bearings and joints is 15.77 kg per vehicle side. The additively manufactured components have a mass of 10.12 kg per vehicle side, which corresponds to a weight reduction of 35.8% with a significant increase in rigidity.

Table 12. Final component weights without bearings and joints.

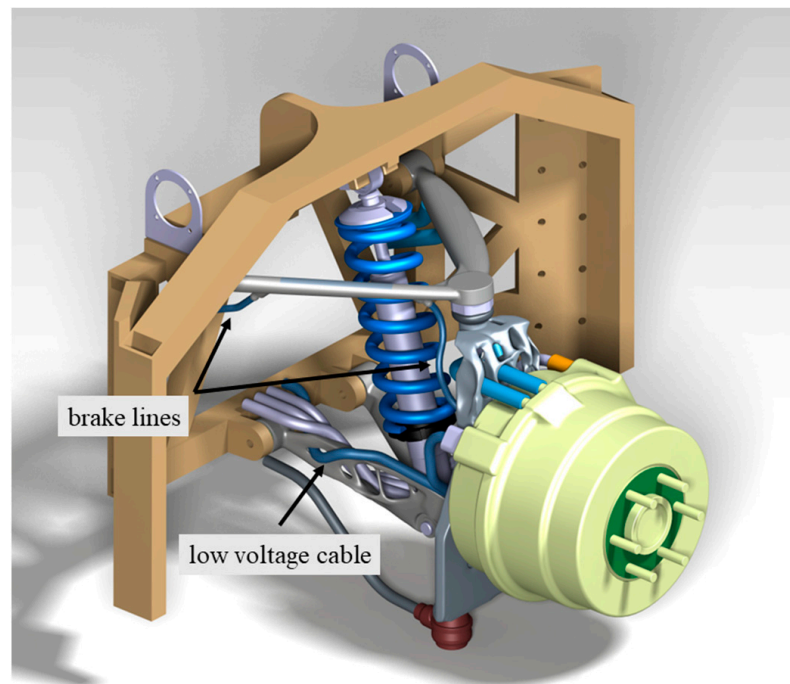| Part	Density [g/cm^3]	Weight [g]
Steering knuckle	4.42	6284
Lower wishbone	4.42	2286
Upper wishbone	2.68	1547

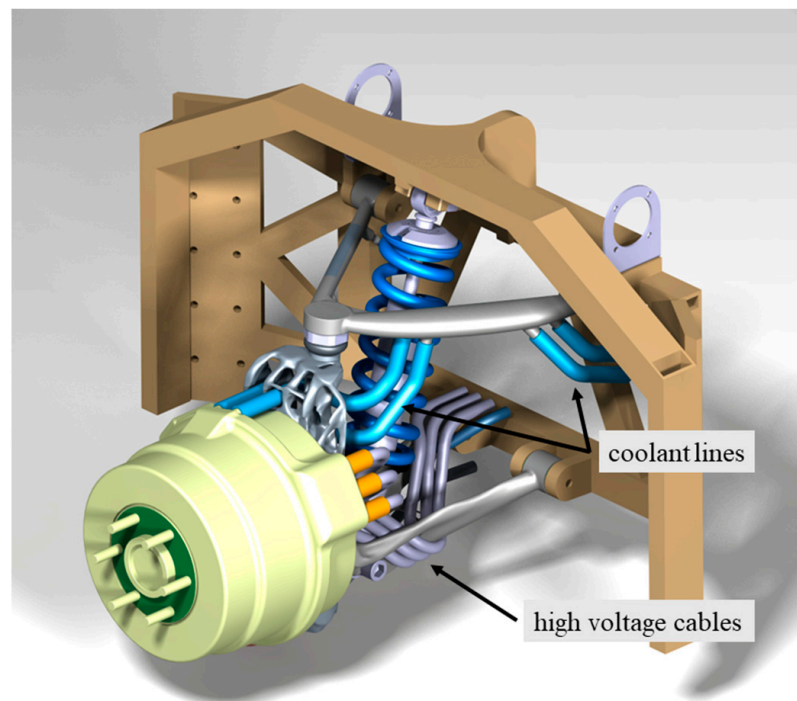**Figure 16.** Entire front-axle suspension system, in front view.

Figure 17. Entire front-axle suspension system in the back view.

4. Summary/Conclusions

This paper deals with the question of how the design freedom of the AM can be used sensefully to optimise a front-axle wheel suspension. In particular, the optimisation of the package through increased functional integration and the lightweight construction aspect are the focus. Using several components, it is shown that the geometric freedoms from additive manufacturing synergise excellently with numerically determined, and thus complex, component geometries. By taking additional functions into account at an early stage of product development, a wide range of problems can be addressed.

Three different approaches to the design of AM suspension components are shown:

- Using the lower wishbone as an example, it is shown that in certain cases, the selection of a suitable optimisation setup for topology optimisation can result in component geometries that are suitable for the integration of a few additional functions. In doing so, the best possible degree of lightweight construction is achieved at the component level.
- In the case of the steering knuckle, the required bushings are already mapped in the design space before optimisation. Due to the static position of the bushings, a medium degree of lightweight construction is achieved, but all the necessary functions are safely fulfilled.
- Using the example of the upper wishbone, it is shown to what extent topology optimisation can be used to identify force-flow paths. Functional integration is achieved for this component by subsequent modelling lines. This procedure is suitable for highly functional components whose individual masses are of medium importance. When viewed holistically, mass is saved through sensible integration at the system level.

The upper wishbone is designed to be force-flow compatible, but it is not ensured that the component mass is minimal in this design. In a further step, the material-carrying lines can be defined as non-design areas, and an optimisation of the surrounding material can be carried out. As a result of the choice of suitable wall thicknesses, further stress homogenisation can be achieved.

It is also recommended to carry out a mesh study on a more powerful computer to validate the FEA results. This allows singularities to be identified and further investigated using fracture-mechanics methods. By producing component prototypes, it is possible to check whether the existing design is suitable for additive manufacturing. The component design can then be further optimised based on these findings. It is also conceivable to specify the component orientation during the building process as a boundary condition for topology optimisation.

Furthermore, the use of bleed nipples in the upper wishbone for easier filling of the brake system must be considered. In order to simplify the fixation of the electrical conductors, the modelling of cable holders is also envisaged.

Conflicts of Interest: The authors declare no conflict of interest.

Definitions/Abbreviations

AM	additive manufacturing
MINDIM	minimum member size
MAXDIM	maximum member size
FEM	finite element method
CAD	computer-aided design
S_{FEM}	safety required due to simplifications in the simulation
SLM	Selective laser melting

References

1. BMVI; Infas; DLR; IVT; Infas 360. Mobilität in Deutschland—MiD: Ergebnisbericht. Bonn, Berlin. 2018. Available online: https://www.mobilitaet-in-deutschland.de/archive/pdf/MiD2017_Ergebnisbericht.pdf (accessed on 23 June 2023).
2. Deutsches Zentrum für Luft- und Raumfahrt e.V. Projekt U-Shift II (Demonstrator). Picture: DLR, CC-BY-ND. Available online: https://verkehrsforschung.dlr.de/de/projekte/u-shift/u-shift-ii-demonstrator (accessed on 23 June 2023).
3. Ersoy, M.; Gies, S. (Eds.) *Fahrwerkhandbuch: Grundlagen, Fahrdynamik, Fahrverhalten, Komponenten, Elektronische Systeme, Fahrerassistenz, Autonomes Fahren, Perspektiven*, 5th ed.; Springer Vieweg: Wiesbaden, Germany, 2017. [CrossRef]
4. Diegel, O.; Nordin, A.; Motte, D. *A Practical Guide to Design for Additive Manufacturing*; Springer: Singapore, 2020. [CrossRef]
5. Lachmayer, R.; Rettschlag, K.; Kaierle, S. (Eds.) *Konstruktion Für Die Additive Fertigung 2020*, 1st ed.; Springer: Berlin/Heidelberg, Germany, 2020. [CrossRef]
6. Carl Hirschmann GmbH. Trag- und Führungsgelenke-Was früher nur auf Anfrage Gefertigt Wurde, ist nun im Standardsortiment Verfügbar. Available online: https://www.carlhirschmann.de/de/Gelenklager/Produktdatenbank/Trag-und-Fuehrungsgelenke-Groesse-16 (accessed on 23 June 2023).
7. EOS GmbH. EOS Titanium Ti64 Grade 5 Material Data Sheet. München. 2019. Available online: https://www.eos.info/03_system-related-assets/material-related-contents/metal-materials-and-examples/metal-material-datasheet/titan/ti64/material_datasheet_eos_titanium_ti64_grade5_en_web.pdf (accessed on 23 June 2023).
8. Debnar, C.S. Geometrieoptimierung und Konstruktion einer Radaufhängung aus Additiver Fertigung. Bachelor's Thesis, Karlsruher Institut für Technologie, Karlsruhe, Germany, 2022.
9. Altair Engineering, Inc. *Practical Aspects of Structural Optimization with Altair OptiStruct*; Big Beaver: Troy, MI, USA, 2021.
10. EOS GmbH. EOS Aluminium AlSi10Mg Material Data Sheet. München. 2022. Available online: https://www.eos.info/03_system-related-assets/material-related-contents/metal-materials-and-examples/metal-material-datasheet/aluminium/material_datasheet_eos_aluminium-alsi10mg_en_web.pdf (accessed on 23 June 2023).
11. Breuer, B.; Bill, K.H. (Eds.) *Bremsenhandbuch: Grundlagen, Komponenten, Systeme, Fahrdynamik*, 5th ed.; Springer Vieweg: Wiesbaden, Germany, 2017. [CrossRef]
12. Gomeringer, R.; Kilgus, R.; Menges, V.; Oesterle, S.; Rapp, T.; Scholer, C.; Stenzel, A.; Stephan, A.; Wieneke, F. *Tabellenbuch Metall: Mit Formelsammlung*, 47th ed.; Verlag Europa-Lehrmittel Nourney Vollmer GmbH & Co. KG: Haan-Gruiten, Germany, 2018.